Geometric Algebra in Quantum Computational Intelligence

Eduardo
Bayro-Corrochano
Institute of Robotics and
Automation
Poznan University of
Technology
Poznan, Poland
eduardo.bayro@put.poznan.pl

ABSTRACT

Recent advancements in artificial intelligence (AI), machine learning, and quantum computing have positioned quantum machine learning as a transformative field. Quantum computers offer a significant advantage in solving complex problems that are difficult for classical systems, by leveraging quantum algorithms for more efficient computations. These developments open up vast possibilities across a wide range of disciplines. In traditional quantum mechanics, the tensor product is employed to construct multiparticle states and define operators acting on them, serving as a tool to distinguish the Hilbert spaces of individual particles. Alternatively, the geometric algebra framework offers an innovative approach to representing the tensor product through the geometric product, utilizing multivectors. In this paper, we introduce several advanced algorithms, including the Quantum Quaternion Fourier Transform, Quantum Key Distribution, Geometric Algebra Quantum Convolutional Neural Networks, and the Geometric Fuzzy Inference Engine, aimed at enhancing robotic decision-making processes.

Keywords

Quantum Computing, Machine Learning, Geometric Algebra, medical image processing, Quantum Key distribution and Robotics

1 INTRODUCTION

Unlike tensor products, which lack an intuitive geometric interpretation, the geometric product and k-vectors (such as points, lines, planes, and volumes) provide a more natural and visualizable framework. Within this context, entangled quantum states can be reinterpreted as k-vectors, representing structured assemblies of geometric entities, including vectors, planes, volumes, hyperplanes, and hypervolumes. For a comprehensive treatment of quantum theory through the lens of geometric algebra, readers are referred to Geometric Algebra Applications Vol. III: Integral Transforms, MachineLearning, and Quantum Computing by E. Bayro-Corrochano (Springer Verlag, 2024).

Quantum machine learning is an emerging interdisciplinary field that merges quantum computing with machine learning techniques. In this lecture, we investigate the foundational principles of quantum machine learning within the geometric algebra framework. Additionally, we present advanced algorithmic approaches, including the Quantum Quaternion Fourier Transform, Geometric Algebra Quantum Convolutional Neural Networks, and the Geometric Fuzzy Inference Engine, with applications in robotic decision-making.

2 GATES IN GEOMETRIC ALGEBRA

Our goal is to use neural networks with neurons that represent gates acting on n-qubits and working in the geometric algebra framework [2, 6]. Thus, we need first to formulate a convenient universal set of quantum gates and then implement them as processing units of neural networks. According to [10], a set of quantum gates $\{\hat{U}_i\}$ is seen as universal if any logical operator \hat{U}_L can be written as

$$\hat{U}_L = \prod_{\hat{U}_L \in \{\hat{U}_i\}} \hat{U}_l. \tag{1}$$

Next, according to the proposed formulations by [4, 6], we will represent simple circuit models of quantum computation with 1-qubit quantum gates in the geometric algebra framework. This subsection is based on the work of Cafaro and Mancini [4].

2.1 The 2-Qubit Space-Time Algebra

Cafaro and Mancini [4] described the 2-Qubit STA; for the sake of completeness, we describe it as well. In the 2-particle algebra there are two bivectors, Ie_3^1 and Ie_3^2 , playing the role of $i_{\mathbb{C}}$. The 2-particle spin states in $B_{[G_3^+ \otimes G_3^+]/E}$ As illustration, the entangled state between

a pair of 2-level systems, called a *spin singlet state*, is formulated as follows:

$$|\psi_{singlet}\rangle = \frac{1}{2} \left\{ \begin{pmatrix} 1 \\ 0 \end{pmatrix} \otimes \begin{pmatrix} 0 \\ 1 \end{pmatrix} - \begin{pmatrix} 0 \\ 1 \end{pmatrix} \otimes \begin{pmatrix} 1 \\ 0 \end{pmatrix} \right\} = \frac{1}{\sqrt{2}} (|01\rangle - |10\rangle) \in \mathbb{H}_{2}^{2}.$$
 (2

$$|\psi_{singlet}\rangle \in \mathbb{H}_2^2 \leftrightarrow \psi_{singlet}^{GA} \in [G_3^+ \otimes G_3^+],$$
 (3)

where

$$\psi_{singlet}^{GA} = \frac{1}{2^{\frac{3}{2}}} (Ie_2^1 - Ie_2^2) (1 - Ie_3^1 Ie_3^2). \tag{4}$$

Following the work of Cafaro and Mancini [4], the multiplication by the quantum imaginary $i_{\mathbb{C}}$ for 2-particle states is taken by the multiplication with J from the right.

$$J = EIe_3^1 = EIe_3^2 = \frac{1}{2}(Ie_3^1 + Ie_3^2). \tag{5}$$

Henceforth $J^2 = -E$. The action of 2-particle Pauli operators reads

$$\hat{\sum}_k \otimes \hat{I} | \psi > \leftrightarrow -Ie_k^1 \psi J, \ \hat{\sum}_k \otimes \hat{\sum}_l | \psi > \leftrightarrow -Ie_k^1 Ie_l^2 \psi E, \ \hat{I} \otimes \hat{\sum}_k | \psi > \leftrightarrow -Ie_k^2 \psi J.$$

2.2 Quantum *NOT* Gate (or Bit Flip Quantum Model)

A nontrivial reversible operation applied to a single qubit is done by means of the NOT operation gate denoted here by $\hat{\Sigma}_1$. Let us apply a 1-qubit quantum gate given by $\psi_{|q}^{GA} = a_0 + a_2 I e_2$. Then, the $\hat{\Sigma}_1$ is defined as

$$\hat{\sum}_1|q>\stackrel{\mathtt{def}}{=}|q\oplus 1> \leftrightarrow \psi_{|q\oplus 1>}^{GA}\stackrel{\mathtt{def}}{=}e_1(a_0+a_2Ie_2)e_3.$$

Since $Ie_i = e_i I$ and $e_i e_j = e_i \land e_j$, we obtain

$$\hat{\sum}_1 |q>\stackrel{\mathtt{def}}{=}|q\oplus 1> \leftrightarrow \pmb{\psi}_{|q\oplus 1>}^{GA} = -(a_2+a_0Ie_2).$$

The action of the unitary quantum gate $\hat{\Sigma}_1^{GA}$ on the basis $\{1, Ie_1, Ie_2, Ie_3\} \in G_3^+$ is as follows:

$$\begin{split} \hat{\sum}_{1}^{GA}: 1 \rightarrow -Ie_{2}, \hat{\sum}_{1}^{GA}: Ie_{1} \rightarrow Ie_{3}, \hat{\sum}_{1}^{GA}: Ie_{2} \rightarrow \\ -1, \hat{\sum}_{1}^{GA}: Ie_{3} \rightarrow Ie_{1}. \end{split}$$

2.3 Quantum Phase Flip Gate

The reversible operation to a single qubit is the phase flip gate denoted by $\hat{\Sigma}_3$. In the GA framework, the action of the unitary quantum gate $\hat{\Sigma}_3^{GA}$ on the multivector $\psi_{|q|}^{GA}=a_0+a_2Ie_2$ is given by

$$\hat{\sum}_{3}|q> \stackrel{\text{def}}{=} (-1)^{q}|q> \leftrightarrow \psi_{(-1)^{q}|q>}^{GA} \stackrel{\text{def}}{=}$$

$$= e_{3}(a_{0}+a_{2}Ie_{2})e_{3}$$

$$= a_{0}-a_{2}Ie_{2}.$$

The unitary quantum gate $\hat{\Sigma}_3^{GA}$ acts on the basis $\{1, Ie_1, Ie_2, Ie_3\} \in G_3^+$ as follows

$$\begin{split} \hat{\sum}_3^{GA}: 1 \rightarrow 1, \hat{\sum}_3^{GA}: Ie_1 \rightarrow -Ie_1, \hat{\sum}_3^{GA}: Ie_2 \rightarrow \\ -Ie_2, \hat{\sum}_3^{GA}: Ie_3 \rightarrow Ie_3. \end{split}$$

2.4 Quantum Bit and Phase Flip Gate

A combination of two reversible operations, $\hat{\Sigma}_1^{GA}$ and $\hat{\Sigma}_3^{GA}$ results in another reversible operation to be applied on a single qubit. This will be denoted by $\hat{\Sigma}_2 \stackrel{\text{def}}{=} i_{\mathbb{C}} \hat{\Sigma}_1 \circ \hat{\Sigma}_3$ and its action on $\psi_{|q>}^{GA} = a_0 + a_2 I e_2$ is given by

$$\begin{split} \hat{\sum}_2 |q> &\stackrel{\text{def}}{=} i_{\mathbb{C}}(-1)^q |q\oplus 1> \leftrightarrow \psi_{(-1)^q|q\oplus 1>}^{GA} \stackrel{\text{def}}{=} \\ e_2(a_0+a_2Ie_2)e_3 &= (a_2-a_0Ie_2)Ie_3. \end{split}$$

The unitary quantum gate $\hat{\Sigma}_2^{GA}$ acts on the basis $\{\Phi, Ie_1, Ie_2, Ie_3\} \in G_3^+$ as follows

$$\begin{split} \hat{\sum}_{2}^{GA}: 1 \rightarrow Ie_{1}, \hat{\sum}_{2}^{GA}: Ie_{1} \rightarrow 1, \hat{\sum}_{2}^{GA}: Ie_{2} \rightarrow \\ Ie_{3}, \hat{\sum}_{2}^{GA}: Ie_{3} \rightarrow Ie_{2}. \end{split}$$

2.5 Hadamar Quantum Gate

The GA formulation of the Walsh-Hadamard quantum gate $\hat{H} \stackrel{\text{def}}{=} \frac{\hat{\Sigma}_1 + \hat{\Sigma}_3}{\sqrt{2}}$ named \hat{H}^{GA} acts on $\psi_{|q>}^{GA} = a_0 + a_2 I e_2$ as follows

$$\begin{split} \hat{H}|q> & \stackrel{\text{def}}{=} \frac{1}{\sqrt{2}}[|q\oplus 1> + (-1)^q|q>]\\ & \leftrightarrow \psi_{\hat{H}|q}^{GA} \stackrel{\text{def}}{=} \left(\frac{e_1+e_3}{\sqrt{2}}\right)(a_1+a_2Ie_2)e_3\\ & = \frac{a_0}{\sqrt{2}}(1-Ie_2) - \frac{a_2}{\sqrt{2}}(1+Ie_2). \end{split}$$

The Hadamard transformations of the states, |+> and |-> are given as follows:

$$|+> \stackrel{\mathsf{def}}{=} \frac{|0>+|1>}{\sqrt{2}} \leftrightarrow \psi_{|+>}^{GA} = \frac{1-Ie_2}{\sqrt{2}}, \ |-> \stackrel{\mathsf{def}}{=} \frac{|0>-|1>}{\sqrt{2}} \leftrightarrow \psi_{|->}^{GA} = \frac{1+Ie_2}{\sqrt{2}}.$$

The unitary quantum gate \hat{H}^{GA} acts on the basis $\{1, Ie_1, Ie_2, Ie_3\} \in G_3^+$ as follows

$$\hat{H}^{GA}: 1 o rac{1 - Ie_2}{\sqrt{2}}, \; \hat{H}^{GA}: Ie_1 o rac{-Ie_1 + Ie_3}{\sqrt{2}}, \ \hat{H}^{GA}: Ie_2 o -rac{1 + Ie_2}{\sqrt{2}}, \hat{H}^{GA}: Ie_3 o rac{Ie_1 + Ie_3}{\sqrt{2}}.$$

2.6 Rotation Quantum Gate

The action of rotation gates \hat{R}^{GA}_{θ} acts on $\psi^{GA}_{|q>}=a_0+a_2Ie_2$ as

follows

$$\begin{split} \hat{R}_{\theta}|q> &\stackrel{\text{def}}{=} \Big(\frac{1+\exp(i_{\mathbb{C}\theta})}{2} + (-1)^q \frac{1-\exp(i_{\mathbb{C}\theta})}{2}\Big)|q> \\ \leftrightarrow \psi_{\hat{R}_{\theta}|q}^{GA} &\stackrel{\text{def}}{=} a_0 + a_2 Ie_2(\cos\theta + Ie_3\sin\theta) \end{split}$$

The unitary quantum gate \hat{R}^{GA}_{θ} acts on the basis $\{1, Ie_1, Ie_2, Ie_3\} \in G_3^+$ in the following manner:

$$\hat{R}_{\theta}^{GA}: 1 \to 1, \ \hat{R}_{\theta}^{GA}: Ie_1 \to Ie_1(\cos\theta + Ie_3\sin\theta),$$

 $\hat{R}_{\theta}^{GA}: Ie_2 \to Ie_2(\cos\theta + Ie_3\sin\theta), \ \hat{R}_{\theta}^{GA}: Ie_3 \to Ie_3.$

Table 2 presents a summary of the most relevant quantum gates in the geometric algebra framework to act on the basis states $\{1, Ie_1, Ie_2, Ie_3\} \in G_3^+$.

1 - QubitState	N	PF	BPF
1	$-Ie_2$	1	Ie_1
Ie ₁	Ie ₃	$-Ie_1$	1
Ie ₂	-1	$-Ie_2$	Ie ₃
Ie ₃	Ie_1	Ie ₃	Ie_2

Table 1: Quantum gates act on the basis states $\{1, Ie_1, Ie_2, Ie_3\} \in G_3^+$, NOT (N), Phase Flip (PF), Bit and Phase Flip (BPF).

1 - QubitState	Hadamard	Rotation
1	$\frac{1-Ie_2}{\sqrt{2}}$	1
Ie ₁	$\frac{-Ie_1+Ie_3}{\sqrt{2}}$	$Ie_1(\cos\theta + Ie_3\sin\theta)$
Ie_2	$-\frac{1+Ie_2}{\sqrt{2}}$	$Ie_2(\cos\theta + Ie_3\sin\theta)$
Ie ₃	$\frac{Ie_1+Ie_3}{\sqrt{2}}$	Ie ₃

Table 2: Quantum gates to act on the basis states $\{1, Ie_1, Ie_2, Ie_3\} \in G_3^+$, Hadamar and Rotation.

3 TWO-QUBIT QUANTUM COMPUT-ING

In this subsection, we study simple circuit models with 2-qubit quantum gates using the geometric algebra framework. This subsection is based on the work of Cafaro and Mancini [4].

We will show that the set of maximally entangled 2-qubit Bell states can be represented in geometric algebra. The Bell states are an interesting example of maximally entangled quantum states, and they form an orthonormal basis \mathcal{B}_{Bell} in the product Hilbert space $\mathbb{C}^2 \otimes \mathbb{C}^2 \cong \mathbb{C}^4$. Given the 2-qubit computational basis $\mathcal{B}_c = \{|00>, |01>, |10>, |01>\}$, according to [10] the four Bell states can be constructed in the following way:

$$\begin{split} |0>\otimes|0>\to|\psi_{Bell_1} \stackrel{\text{def}}{=} \left[\hat{U}_{CNOT} \circ (\hat{U} \otimes \hat{I}) \right] (|0>\otimes|0>) = \\ \frac{1}{\sqrt{2}} (|0>\otimes|0>+|1>\otimes|1>), \\ |0>\otimes|1>\to|\psi_{Bell_2} \stackrel{\text{def}}{=} \left[\hat{U}_{CNOT} \circ (\hat{U} \otimes \hat{I}) \right] (|0>\otimes|1>) = \\ \frac{1}{\sqrt{2}} (|0>\otimes|1>+|1>\otimes|0>), \\ |1>\otimes|0>\to|\psi_{Bell_3} \stackrel{\text{def}}{=} \left[\hat{U}_{CNOT} \circ (\hat{U} \otimes \hat{I}) \right] (|1>\otimes|0>) = \\ \frac{1}{\sqrt{2}} (|0>\otimes|0nn>-|1>\otimes|1>), \\ |1>\otimes|1>\to|\psi_{Bell_4} \stackrel{\text{def}}{=} \left[\hat{U}_{CNOT} \circ (\hat{U} \otimes \hat{I}) \right] (|1>\otimes|1>) = \\ \frac{1}{\sqrt{2}} (|0>\otimes|1>-|1>\otimes|0>), \end{split}$$

where \hat{H} and \hat{U}_{CNOT} stand for the Hadamard and the CNOT gates respectively. The Bell basis in $\mathbb{C}^2 \otimes \mathbb{C}^2 \cong \mathbb{C}^4$ is given by

$$\mathscr{B}_{\textit{Bell}} \stackrel{\text{def}}{=} \{|\psi_{\textit{Bell}_1}>, |\psi_{\textit{Bell}_2}>, |\psi_{\textit{Bell}_3}>, |\psi_{\textit{Bell}_4}>\}.$$

According to equation (7), we obtain

$$\begin{split} |\psi Bell_1> &= \frac{1}{\sqrt{2}} \begin{pmatrix} 1\\0\\0\\1 \end{pmatrix}, |\psi Bell_2> = \frac{1}{\sqrt{2}} \begin{pmatrix} 0\\1\\1\\0 \end{pmatrix}, \\ |\psi Bell_3> &= \frac{1}{\sqrt{2}} \begin{pmatrix} 1\\0\\0\\-1 \end{pmatrix}, |\psi Bell_4> &= \frac{1}{\sqrt{2}} \begin{pmatrix} 0\\1\\-1\\0 \end{pmatrix}. \end{split}$$

Using equation (7), the formulation of the Bell states in geometric algebra is as follows:

$$\begin{split} |\psi Bell_1> &\leftrightarrow \psi^{GA}_{Bell_1} = \frac{1}{2^{\frac{3}{2}}}(1+Ie_2^1Ie_2^2)(1-Ie_3^1Ie_3^2)), \\ |\psi Bell_2> &\leftrightarrow \psi^{GA}_{Bell_2} = -\frac{1}{2^{\frac{3}{2}}}(Ie_2^1+Ie_2^2)(1-Ie_3^1Ie_3^2)), \\ |\psi Bell_3> &\leftrightarrow \psi^{GA}_{Bell_3} = \frac{1}{2^{\frac{3}{2}}}(1-Ie_2^1Ie_2^2)(1-Ie_3^1Ie_3^2)), \\ |\psi Bell_4> &\leftrightarrow \psi^{GA}_{Bell_4} = \frac{1}{2^{\frac{3}{2}}}(Ie_2^1-Ie_2^2)(1-Ie_3^1Ie_3^2)). \end{split}$$

3.1 2-Qubit CNOT Quantum Gate

According to [10] a CNOT quantum gate can be written as

$$\hat{U}_{CNOT}^{12} = \frac{1}{2} \left[\left(\hat{I}^1 + \hat{\Sigma}_3^1 \right) \otimes \hat{I}^2 + \left(\hat{I}^1 - \sum_3^1 \right) \otimes \hat{\Sigma}_1^2 \right]$$
 (8)

where \hat{U}_{CNOT}^{12} is the CNOT gate from qubit 1 to qubit 2, thus

$$\hat{U}_{CNOT}^{12}|\psi\rangle = (9)$$

$$\frac{1}{2} \left[\hat{I}^1 \otimes \hat{I}^2 + \hat{\Sigma}_3^1 \otimes \hat{I}^2 + \hat{I}^1 \otimes \hat{\Sigma}_1^2 - \hat{\Sigma}_3^1 \right] \otimes \hat{\Sigma}_1^2 \right] |\psi\rangle.$$

Using equations (10) and (6), it follows

$$\hat{I}^{1} \otimes \hat{I}^{2} | \psi > \leftrightarrow \psi, \ \hat{\sum}_{3}^{1} \otimes \hat{I}^{2} | \psi > \leftrightarrow -Ie_{3}^{1} \psi J,
\hat{I}^{1} \otimes \hat{\sum}_{1}^{2} | \psi > \leftrightarrow -Ie_{1}^{2} \psi J,
-\hat{\sum}_{3}^{1} \otimes \hat{\sum}_{1}^{2} | \psi > \leftrightarrow Ie_{3}^{1} Ie_{1}^{2} \psi E$$
(10)

Now using equation (6), the CNOT gate of equation (10) is formulated in GA as follows:

$$\hat{U}_{CNOT}^{12}|\psi> \leftrightarrow \frac{1}{2}(\psi - Ie_3^1\psi J - Ie_1^2\psi J + Ie_3^1Ie_1^2\psi E). (11)$$

3.2 2-Oubit Controlled-Phase Gate

According to [10], the action of the Controlled Phase gate \hat{U}_{CP}^{12} on $|\psi>\in \mathbb{H}_2^2$ can be formulated as

$$\hat{U}_{CP}^{12}|\psi> = \frac{1}{2} \left[\hat{I}^1 \otimes \hat{I}^2 + \hat{\boldsymbol{\Sigma}}_3^1 \otimes \hat{I}^2 + \hat{I}^1 \otimes \hat{\boldsymbol{\Sigma}}_3^2 - \hat{\boldsymbol{\Sigma}}_3^1 \otimes \hat{\boldsymbol{\Sigma}}_3^2 \right] |\psi>.$$

Using equations (13) and (6), it follows

$$\hat{I}^{1} \otimes \hat{I}^{2} | \psi > \leftrightarrow \psi, \, \hat{\Sigma}_{3}^{1} \otimes \hat{I}^{2} | \psi > \leftrightarrow
-Ie_{3}^{1} \psi J, \, \hat{I}^{1} \otimes \hat{\Sigma}_{3}^{2} | \psi > -Ie_{3}^{2} \psi J,
-\hat{\Sigma}_{3}^{1} \otimes \hat{\Sigma}_{3}^{2} | \psi > \leftrightarrow Ie_{3}^{1} Ie_{3}^{2} \psi E$$
(13)

Using equations (6) and (13), one can formulate in geometric algebra the controlled-phase quantum gate as follows:

$$\hat{U}_{CP}^{12}|\psi\rangle \leftarrow \frac{1}{2}(\psi - Ie_3^1\psi J - Ie_3^2\psi J + Ie_3^1Ie_3^2\psi E). \tag{14}$$

3.3 2-Qubit SWAP Gate

According to [10], the action of the Swap gate \hat{U}_{SWAP}^{12} on $|\psi\rangle \in \mathbb{H}_2^2$ can be formulated as

$$\hat{U}_{SWAP}^{12}|\psi\rangle = \frac{1}{2} \left[\hat{I}^1 \otimes \hat{I}^2 + \hat{\Sigma}_1^1 \otimes \hat{\Sigma}_1^2 + \hat{\Sigma}_2^1 \otimes \hat{\Sigma}_2^2 + \hat{\Sigma}_3^1 \otimes \hat{\Sigma}_3^2 \right] |\psi\rangle.$$
(15)

Using equations (16), it follows

$$\hat{I}^{1} \otimes \hat{I}^{2} | \psi \rangle \leftrightarrow \psi, \ \hat{\sum}_{1}^{1} \otimes \hat{\sum}_{1}^{2} | \psi \rangle \leftrightarrow -Ie_{2}^{1} Ie_{2}^{2} \psi E,$$

$$\hat{\sum}_{2}^{1} \otimes \hat{\sum}_{2}^{2} | \psi \rangle \leftrightarrow -Ie_{2}^{1} Ie_{2}^{2} \psi E, \ \hat{\sum}_{3}^{1} \otimes \hat{\sum}_{3}^{2} | \psi \rangle \leftrightarrow -Ie_{3}^{1} Ie_{3}^{2} \psi E$$

$$(16)$$

Using equation (17), the SWAP quantum gate in GA reads

$$\hat{U}_{SWAP}^{12}|\psi>\leftarrow\frac{1}{2}(\psi-Ie_1^1Ie_1^2\psi E-Ie_1^2Ie_2^2\psi E-Ie_3^1Ie_3^2\psi E).$$

Table 3 summarizes the most important 2-qubit quantum gates formulated in the geometric algebra basis. $\mathcal{B}_{[G_3^+\otimes G_3^+]/E}$

2Q Gat	Gate Action on States
CNOT	$\frac{1}{2}(\psi - Ie_3^1\psi J - Ie_1^2\psi J + Ie_3^1Ie_1^2\psi E)$
CP	$\frac{1}{2}(\psi - Ie_3^1\psi J - Ie_3^2\psi J + Ie_3^1Ie_3^2\psi E)$
SWAP	$\frac{1}{2}(\psi - Ie_1^1 Ie_1^2 \psi E - Ie_1^2 Ie_2^2 \psi E - Ie_3^1 Ie_3^2 \psi E)$

Table 3: 2-Qubit Quantum gates: CNOT, Controlled Phase, and SWAP gates to act on the basis $\mathscr{B}_{[G_3^+\otimes G_3^+]/E}$.

4 QUANTUM COMPUTING FOR COMMUNICATION

Distributing quantum information between remote locations requires the integration of emerging quantum technologies with existing communication infrastructure, [5, 7] Achieving this integration necessitates a thorough understanding of how communication channels degrade transmitted quantum signals, an essential step toward implementing practical solutions for theoretically unconditionally secure key generation. However, current experimental quantum key distribution (QKD) systems, which rely on photon transmission, face limitations due to various hardware imperfections. These non-idealities restrict the overall

performance and scalability of QKD technologies. To advance the engineering of future QKD systems, classical simulations of the optical components used in these systems may play a critical role, going beyond traditional characterization techniques employed in classical communication systems. The main obstacle in longdistance quantum communication remains transmission loss, primarily caused by absorption and scattering in optical fibers or atmospheric channels. While classical systems compensate for such losses with optical amplifiers acting as repeaters, this approach is not viable in quantum systems, as amplifying individual photons would irreversibly destroy the quantum information they carry. Although research into quantum repeaters is ongoing, these technologies are not yet mature enough to support intercontinental quantum communication [11].

In Quantum Communications we deal with teleportation; as an illustration, we present below the implementation for the Bob and Alice problem using Quaternion Algebra.

Bob and Alice Problem

Preparation

If Alice chooses bit $a \in 0, 1$ and base $b \in \{comp, j\}$:

$$|\psi>= \begin{cases} |0>o|1>if b=comp, \\ |b_0>o|b_1>, if b=j \end{cases}$$

depending upon if a = 0 o a = 1.

Intercept-resend (Bob)

If Alice intercepts:

- 1. Chooses base $b_E \in \{comp, j\}$.
- 2. Measures $|\psi\rangle$ in $\mathcal{B}_{b_E}\to$ obtains x_E and collapses to $|e_{x_E}^{(b_E)}>$.
- 3. Resend $|\psi'\rangle = |e_{x_E}^{(b_E)}\rangle$ to Bob.

Program

INPUT: n (number of signals), $p_{Alice} \in [0, 1]$

FOR t = 1..n:

Choices of Alice

 $a_t \leftarrow \text{Bernoulli}(1/2) \# \text{bit}$

 $bA_t \leftarrow \text{choice } \{comp, j\} \text{ # base}$

 $|\psi_t> \leftarrow |a_t>$ in base bA_t.

This means:

if
$$bA_t = comp$$
: $|\Psi_t> = |0> (a_t = 0), o |1> (a_t = 1)$

if
$$bA_t$$
= j : $|\Psi_t>=|b_0>(a_t=0), \, o\,|b_1>(a_t=1)$

Possible Bob Channel

if Uniform $(0,1) < p_{Bob}$:

$$bE_t \leftarrow choice\{comp, j\}$$

measure to Bob in $\mathcal{B}_{\{bE_t\}}$:

$$p_x = || \langle e_x^{\{(bE_t)\}} | \Psi_t \rangle ||^2, x \in \{0, 1\}$$

 $xE_t \approx Categorical(p_0, p_1)$

$$|\Psi_t'> \leftarrow |e)_{\{xE_t\}}^{\{(bE_t)\}} >$$

QUANTUM QUATERNION FAST FOURIER TRANSFORM

The Quaternion Quantum Fourier Transform (QQFT) maps the quaternion quantum set $|x> = \sum_{j=0}^{N-1} x_j |j>$ to the quaternion quantum state $|y\rangle = \sum_{k=0}^{N-1} y_k |k\rangle$, [3]. For the QQFT equation, it is needed to change

the complex exponential of the QFT, with a quaternion exponential as follows

$$|x> = \sum_{j=0}^{N-1} x_j |j> \stackrel{QQFT}{\longrightarrow} |y> = \sum_{k=0}^{N-1} y_k |k>.$$
 (17)

$$|j>=rac{1}{\sqrt{N}}\sum_{k=0}^{N-1}e^{2\pi\murac{jk}{N}}|k>, \ {\it where}, \ \mu=rac{1}{\sqrt{3}}(i+j+k).$$

The Inverse Quaternion Quantum Fourier Transform (IQQFT) is then given by

$$|y> = \sum_{k=0}^{N-1} y_k |k> \xrightarrow{IQQFT} |x> = \sum_{j=0}^{N-1} x_j |j>,$$
 (18)

and

$$|k> = \frac{1}{\sqrt{N}} \sum_{j=0}^{N-1} e^{-2\pi\mu \frac{jk}{N}} |j>, \text{ where, } \mu = \frac{1}{\sqrt{3}} (i+j+k).$$

Or the unitary matrix

$$U_{QQFT} = \frac{1}{\sqrt{N}} \sum_{i=0}^{N-1} \sum_{k=0}^{N-1} w_N^{ik} |k> < j|,$$
 (19)

where $w_N^{ik} = e^{2\pi\mu \frac{jk}{N}}$. As a matrix, the corresponding unitary operator U_{QQFT} is given by

This fliells. # tif bA_t = comp:
$$|\Psi_t> = |0> \ (a_t=0), \ o\ |1>$$

if bA_t = j: $|\Psi_t> = |b_0> \ (a_t=0), \ o\ |b_1>$
 $U_{QQFT}=\frac{1}{\sqrt{N}}\begin{bmatrix} 1 & 1 & 1 & \dots & 1\\ 1 & w_n & w_n^2 & w_n^3 & \dots & w_n^{N-1}\\ 1 & w_n^2 & w_n^4 & w_n^6 & \dots & w_n^{2(N-1)}\\ 1 & w_n^3 & w_n^6 & w_n^9 & \dots & w_n^{3(N-1)}\\ \vdots & \vdots & \vdots & \vdots & \vdots & \vdots\\ 1 & w_n^{N-1} & w_n^{2(N-1)} & w_n^{3(N-1)} & \dots & w_n^{N-1(N-1)} \end{bmatrix},$ ble Bob Channel

where $w_n = e^{\frac{2\pi\mu}{2^n}}$. For the U_{IOOFT} , we use $w_N^{ik} =$ $e^{-2\pi\mu \frac{jk}{N}}$ instead.

Application of the Quaternion Quan-5.1 tum Fast Fourier Transform

Given an RGB f(x,y) image, each pixel can be represented as a pure quaternion as follows:

$$q(x,y) = (0,\vec{q}) = R(x,y)i + G(x,y)j + B(x,y)k$$
 (20)

However, we propose instead to use the following exponential function

$$q(x,y) = e^{\theta n} = \cos(\theta) + n\sin(\theta), \tag{21}$$

where

$$n = \frac{R(x,y)i + G(x,y)j + B(x,y)k}{\sqrt{R(x,y)^2 + G(x,y)^2 + B(x,y)^2}},$$

$$\theta = \sqrt{R(x,y)^2 + G(x,y)^2 + B(x,y)^2}.$$

A quantum quaternion RGB image pixel *x* is represented by two qubits, which is a superposition of four quantum states as follows:

$$x = \alpha_1 |00> +\alpha_2 |01> +\alpha_3 |10> +\alpha_4 |11>, \quad (22)$$
where for $|n| = \sqrt{R(x,y)^2 + G(x,y)^2 + B(x,y)^2},$

$$\alpha_1 = \cos(\theta), \ \alpha_2 = \frac{\sin(\theta)}{|n|} R(x,y)i, \quad (23)$$

$$\alpha_3 = \frac{\sin(\theta)}{|n|} G(x, y) j, \ \alpha_4 = \frac{\sin(\theta)}{|n|} B(x, y) k,$$

where $\sum_{n=1}^{4} \alpha_n^2 = 1$.

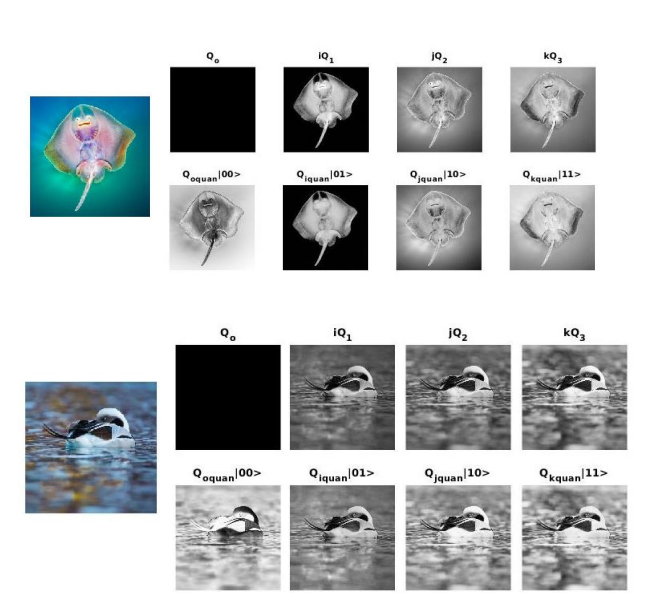


Figure 1: RGB images represented as quaternion quantum images

Figure 1 shows two RGB images as quaternion quantum images. Since we can not use convolution to compute the filtering of quantum images, we should simply filter the quaternion quantum image in the frequency domain by using constraints to delimit the band of the image in question.

To filter in the frequency domain, firstly we have to transform the quaternion quantum image using the Quaternion Quantum Fast Fourier Transform. In this work, we are not using a quantum computer, but to speed up the Quaternion Fourier Transform, we use the Fast Fourier Transform (FFT). Figure 2 presents the Quaternion Quantum Fast Fourier Transform of an RBG image and the Inverse Quaternion Quantum Fast Fourier Transform.

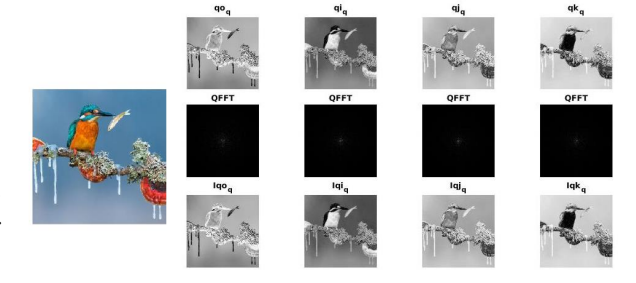


Figure 2: Quaternion Quantum Fast Fourier Transform and its inverse of an RGB image, according to equations (17) and (18)

6 QUANTUM COMPUTING AND MA-CHINE LEARNING FOR IMAGE PROCESSING, ARCHITECTURE

As shown in Figure 3, we introduce a hybrid quantum classical convolutional neural network architecture, designated the Geometric (Clifford) QuanConvolutional Neural Network (CQCNN) [8, 9], for advanced feature extraction in medical image analysis [1]. This architecture synergistically integrates the representational power of quantum convolution, quaternion convolution [6], and Clifford convolution, enabling the preservation of multi-channel geometric correlations while leveraging quantum-enhancedfeature embeddings. The CQCNN is designed for medical image analysis tasks where local geometric structure is diagnostically significant.

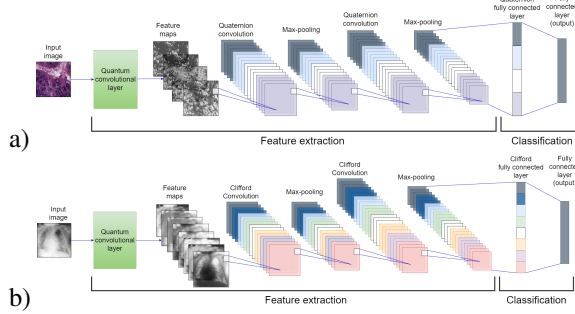


Figure 3: a) Architecture of the Quaternion Quanvolutional Neural Network. b) Architecture of the Geometric (Clifford) Quanvolutional Neural Network.

The architecture of the Quaternion Quanvolutional Neural Network QCNNs are extended to QQNNs by adding a quanvolutional layer. By applying a quanvolutional layer (with a 4-qubit circuit) to an RGB (or a grayscale) input image we obtain four latent space features that are subsequently processed by a QQCNN;see Figure 3. The last layer corresponds to a ffully connectedlayer with a softmax function used for classification. The architecture of the Geometric (Clifford) Quanvolutional Neural Network: GCNNs

are extended to GQNNs by adding a quanvolutional layer.

Quantum Convolutional Layer

Let $I \in \mathbf{R}^{H \times W \times C}$ represent the input image, where H, W and C denote height, wwidth,and number of channels, respectively. The quantum convolutional layer operates as follows:

1. **Patch Encoding**: The image is divided into nonoverlaping patches P_k of size $p \times p$, which are encoded into a quantum state

$$|\psi_k>=U_{enc}(P_k)|0>^{\otimes n_q}$$

where U_{enc} is the parameterized encoding unitary and n_q is the number of qubits.

2. **Quantum Convolution**: A parameterized quantum circuit PQC U_{θ} processes the eencodedstates:

$$|\phi_k > U_\theta|\psi_k >$$

3. **Measurement**: Expectation values of observables O_i yield the feature maps:

$$f_{k,i} = \langle \phi_k | O_i | \phi_k \rangle, i = 1, ..., n_k$$

Thus, each path yields n_k scalar features, producing quantum-generated feature maps $F^{(Q)} \in \mathbf{R}^{H^t \times W^t \times n_q}$.

Geometric (Clifford) Algebra Quantum Convolutional Layer

The output feature maps from the quantum layer are processed collectively within a geometric algebra framework $G_{p,q}$, allowing the representation of vectors, bivectors, and high-grade geometric entities.

Given the quantum feature maps $F^{(Q)}$, one forms a multivector representation:

$$M(x,y) = \sum_{i=1}^{n_q} f_{x,y,i} e_i$$

where e_i are the orthogonal basis elements of the geometric algebra.

A Ggeometric algebra convolution kernel K of size $k \times k$ acts via the geometric product

$$(M*K)(x,y) = \sum_{u=-|k/2|}^{k/2} \sum_{v=-|k/2|}^{k/2} M(x+u,y+v)K(u,v).$$

This convolution inherently preserves orientation, phase, and multidimensional correlations, outperforming scalar convolutions in rotational and geometric invariance.

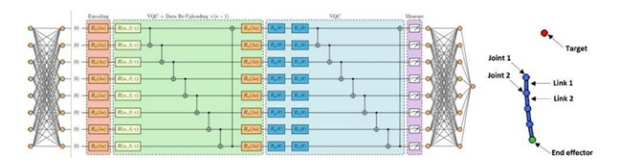


Figure 4: Variational Quantum Soft Actor-Critic to control the movement of a robotic arm

7 QUANTUM REINFORCEMENT LEARNING FOR CONTINUOUS CONTROL

Figure 4 shows a Variational Quantum Soft Actor-Critic to control the movement of a robotic arm. We propose to enhance the Soft Actor-Critic (SAC) algorithm for continuous robotic control tasks by incorporating quantum computing techniques, resulting in a Variational Quantum Soft Actor-Critic (VQ-SAC) framework. The aim is to investigate whether variational quantum circuits can improve exploration efficiency and learning speed, addressing two key bottlenecks in real-world reinforcement learning (RL):

- i. Exploration Strategy avoiding inefficient or myopic exploration in large continuous action spaces.
- ii. Curse of Dimensionality mitigating slow convergence in high-dimensional state-action spaces. The approach will be evaluated in the context of robotic arm movement control, using simulated and real-time systems.

8 QUANTUM GEOMETRIC FUZZY INFERENCE ENGINES FOR DECI-SION TAKING IN ROBOTICS

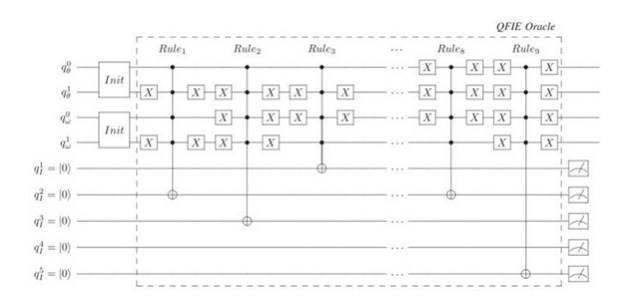


Figure 5: Quantum Fuzzy Inference Engine

The design of a Quantum Fuzzy Inference Engine (QFIE) accomplishes a twofold objective. First, it delivers an exponential speedup in the execution of fuzzy rules compared to a classical oracle-based fuzzy inference engine, by exploiting quantum parallelism and amplitude encoding of fuzzy membership degrees. Second, it opens a novel avenue for quantum programming via fuzzy linguistic rules, providing an intuitive, high-level framework for defining quantum

algorithms in terms familiar to engineers and domain experts. This paradigm makes it possible to describe decision processes for quantum computers using the approximate reasoning capabilities inherent to fuzzy logic, while leveraging quantum computational speedups. Figure 5 shows the implemented circuit, where a measurement operation on each qubit of QRI is added after the implementation of the oracle. This combination of quantum information processing, quantum Fuzzy Finite State Machine, fuzzy logic reasoning, and geometric modeling holds potential for a new class of intelligent control systems that are both computationally efficient and linguistically interpretable, suitable for complex real-time applications in robotics, autonomous systems, and adaptive control. Next we present the implementation of the Quantum Oracle for Fuzzy Encoding and the Quantum Fuzzy Finite State Machines Representations.

Quantum Oracle for Fuzzy Rule Encoding

The Ffuzzyrule base has the general form:

$$R_j$$
: **IF** θ is A_j **AND** w is B_j **THEN** I is C_j

In **QFIE**, the oracle O_f encodes the mapping:

$$O_f: |A_i| > |B_i| > |0| > \rightarrow |A_i| > |B_i| > |C_i| >$$

This is implemented as a controlled unitary:

$$O_f = \sum_{A|B} |A>$$

where U_{AB} maps the output register from |O> to the state representing the consequent C with amplitudes proportional to the minimum (or another t-norm) of the antecedent memberships:

$$U_{AB}|0> = \frac{1}{\sqrt{\sum_{c}\alpha_{c}^{2}}}\sum_{c}\alpha_{c}|c>, \ \alpha_{c} = \min(\mu_{A}(\theta), \mu_{B}(w))$$

Because all rules are evaluated in quantum superposition, the complexity is reduced compared to sequential evaluation.

Quantum Fuzzy Finite State Machine Representation

The system's dynamics can be represented by a Quantum Fuzzy Finite State Machines (QFFSM)

$$|\psi(t+1)>=U|\psi(t)>$$

where U_f is a fuzzy-weighted unitary transition operator, defined as:

$$U_f = \sum_{s,s'} \Lambda |s'> < s|$$

with fuzzy transition amplitudes $\Lambda_{s,s'} \in [0,1]$ satisfying unitary constraints.

9 CONCLUSION

In traditional quantum mechanics, the tensor product is employed to construct multiparticle states and define operators acting on them, serving as a tool to distinguish the Hilbert spaces of individual particles. In contrast, the Ggeometric algebraframework offers an innovative approach for representing the tensor product through the geometric product, utilizing multivectors. In this paper, we have introduced several advanced algorithms, including the Quantum Quaternion Fourier Transform, Quantum Key Distribution, Geometric Algebra Quantum Convolutional Neural Networks, and the Geometric Fuzzy Inference Engine, aimed at enhancing robotic decision-making processes.

10 REFERENCES

- [1] Altamirano-Escobedo G. E. Bayro-Corrochano. 2023. Geometric Algebra Quantum Convolutional Neural Network: A model using geometric (Clifford) algebras and quantum computing. Hypercomplex Signal and Image Processing. IEEE Signal Processing Magazine, vol. 41, no. 2, pp. 75-85.
- [2] Bayro-Corrochano, E. 2024. Geometric Algebra Applications Vol. III: Inte-gral Transforms, Machine Learning, and Quantum Computing. Springer Nature, Switzerland.
- [3] Bayro-Corrochano, E. Vazquez-Flores, Z. . 2023. Image processing using the quantum quaternion Fourier transform. Mathematical Methods in Applied Sciences, Volume 47, Issue3, Pages 1305-1317.
- [4] Cafaro C. and Mancini S. . 2010. A geometric algebra perspective on quantum computational gates and universality in quantum computing. arXiv:1006.2071v1 [math-ph] 10 June.
- [5] Caputo, M.S., Giovanni, A.C., Giovanna, T. and Maurizio, Z. 2022. A simulator of optical coherent-state evolution in quantum key distribution systems. Optical and Quantum Electronics, 54:689, https://doi.org/10.1007/s11082-022-04041-8.
- [6] Chappell J.M. . 2011. Quantum Computing, Quantum Games and Geometric Algebra. PhD Thesis, The School of Chemestry amd Physics, University of Adelaide, Australia.
- [7] Gupta, S. et al. 2025 Robust simulation of continuous-variable quantum key distribution in Matlab and Simulink. Academia Quantum, 2025(2), pp. 1 of 14, https://doi.org/10.20935/AcadQuant7844.
- [8] Henderson, M., Shakya, S., Pradhan, S. and Tristan, C. 2020. Quanvolutional neural networks: powering image recognition with quantum circuits. Quantum Machine Intelligence, Vol. 2(1), pp. 1-9, Springer.
- [9] Gaudet, Chase J and Maida, Anthony S. 2018 Deep quaternion networks. 2018 International Joint Conference on Neural Networks (IJCNN), pp. 1-8.
- [10] Nielsen A. and Chuang I. L. . 2000. *Quantum Computation and Information*, Cambridge Press.
- [11] Yin, J. et al. 2017. Satellite-based entanglement distribution over 1200 kilometers. Science 356, 1140